PERGAMON

International Journal of Solids and Structures 36 (1999) 2485–2505

INTERNATIONAL JOURNAL OF SOLIDS and STRUCTURES

# Tilting stiffness of elastic layers bonded between rigid plates

Hsiang-Chuan Tsai*, Chung-Chi Lee

*Department of Construction Engineering, National Taiwan University of Science and Technology, P.O. Box 90-130, Taipei, Taiwan, R.O.C.*

Received 9 January 1997; in revised form 14 March 1998

**Abstract**

A theoretical approach to determine the tilting stiffness of an elastic layer bonded between rigid plates is presented and then applied to derive the formulae of tilting stiffness for layers of infinite-strip, circular and square shapes. Based on two kinematics assumptions, the governing equations for the mean pressure are established from the equilibrium equations and the bulk modulus equation. Satisfying the stress boundary conditions, the pressure functions are solved and the formulae for tilting stiffness are derived. The tilting stiffnesses calculated from these formulae are extremely close to the results obtained from the finite element method for an extensive range of shape factor and Poisson's ratio. 

## 1. Introduction

The technique of laminated elastomeric bearing has many uses in structural design, such as thermal expansion bearings for highway bridges and isolated bearings to reduce seismic response of buildings. A laminated elastomeric bearing consists of sheets of elastomer bonded to interleaving steel plates. When an elastic layer is bonded between two rigid plates, the restricted lateral expansion of the bonded surfaces of the elastic layer results in higher compression stiffness than an unbonded elastic layer. Thus, laminated elastomeric bearing provides high vertical rigidity to sustain gravity loading, while still providing the same horizontal flexibility of an unbonded elastomer.

Using approximate theoretical analyses, Gent and Lindley (1959) derived the compressive stiffness of an incompressible elastic layer bonded between rigid plates for infinite-strip shape and circular shape. Subsequently, Gent and Meinecke (1970) extended this method to analyze the compressive stiffness and tilting stiffness of incompressible elastic layers for square and other shapes. These approximate analyses are based on two kinematics assumptions and one stress assumption, which are (i) planes parallel to the rigid bonding plates before deformation remain

* Corresponding author. Fax: 00 886 2 2737 6606.

0020–7683/99/$ - see front matter 
PII: S0020–7683(98)00119–X

planar after loading; (ii) lines normal to the rigid bonding plates before deformation become parabolic after loading; (iii) the normal stress components in all three directions can be approximated by the mean pressure. The solutions are obtained from the superposition of two stages: (i) the elastic layer is first deformed between unbonded rigid plates; (ii) shear stresses are then applied to restore the top and bottom surfaces of the elastic layer to the bonded positions.

Although rubber can be treated as incompressible in some analyses, the assumption of incompressibility tends to overestimate the compressive stiffness and tilting stiffness of the bonded rubber layer when the layer's shape factor (defined as the ratio of the one bonded area to the force-free area) is high. Kelly (1993) developed a theoretical approach to derive the compressive stiffness and tilting stiffness considering the effect of bulk compressibility. Based on the above three assumptions and two-stage deformations, the relation between mean pressure and volume strain is reduced to a partial differential equation of the pressure, from which the compressive and tilting stiffnesses, including the influence of volume change, are derived. The solutions, referred to as 'approximate pressure' solutions here, are available for the layers of infinite-strip shape (Chalhoub and Kelly, 1991), circular shape (Chalhoub and Kelly, 1990) and square shape (Koh and Kelly, 1987). These solutions are accurate for layers of high shape factor and a material of Poisson's ratio between 0.49 and 0.5, e.g. rubber.

Lindley (1979a) applied an energy method to derive the compressive stiffness of the infinite-strip and circular shapes as well as the tilting stiffness of the infinite-strip shape (Lindley, 1979b). In addition to the forementioned two kinematics assumptions, he also postulated that the volume strain has a parabolic distribution across the plane of the layer. These solutions are accurate for the material of any Poisson's ratio.

The authors of this paper have developed a pressure approach to derive the compressive stiffness of a bonded elastic layer in infinite-strip, circular and square shapes (Tsai and Lee, 1998). This approach is a direct solution, not a two-stage solution, and relies on the only two kinematics assumptions that horizontal planes remain planar and vertical lines become parabolic after loading. Partial differential equations for the pressure are initially derived from the equilibrium equations and the bulk modulus equation. By satisfying the stress boundary conditions of the layers, the pressure functions are then solved, from which the compressive stiffnesses are derived. The derived compressive stiffnesses are shown to be extremely close to the results of finite element analysis for any value of Poisson's ratio and shape factor. In this paper, we apply the same pressure approach to derive the tilting stiffness of bonded elastic layer of infinite-strip, circular and square shapes and compare the derived results with the finite element solutions and the results published previously.

## 2. Governing equations

A layer of linearly elastic, homogeneous and isotropic material is bonded between two rigid plates as shown in Fig. 1. A rectangular Cartesian coordinate system $(x, y, z)$, is established by locating the origin at the center of the layer and the $xy$ plane in the middle plane of the layer. The layer has a thickness $t$ and an area $A$. Let $u$, $v$ and $w$ represent the displacements in the $x$, $y$ and $z$ coordinate directions, respectively. As shown in Fig. 2, the top and bottom rigid plates rotate about the $y$ axis to form an angle $\phi$. Because the surfaces of the layer are perfectly bonded to rigid

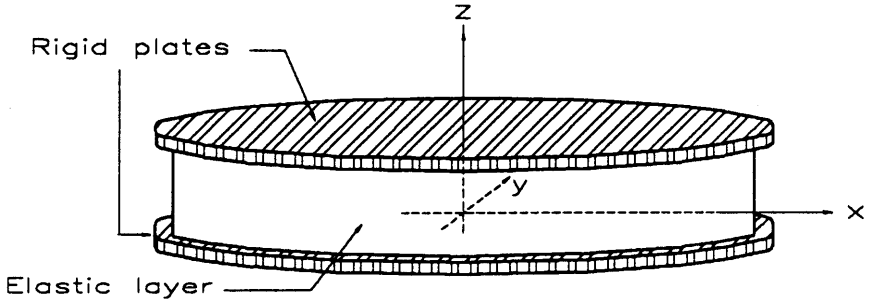


Fig. 1. Elastic layer bonded between rigid plates.

plates, the deformation of the elastic layer is symmetric to the $xy$ plane. The displacements are assumed to have the form

$$u(x,y,z) = \bar{u}(x,y)\left(1-\frac{4z^2}{t^2}\right)-\frac{1}{2\rho}z^2 \tag{1}$$

$$v(x,y,z) = \bar{v}(x,y)\left(1-\frac{4z^2}{t^2}\right) \tag{2}$$

$$w(x,y,z) = \frac{1}{\rho}xz \tag{3}$$

where $\rho = t/\phi$ is the radius of curvature of the rotation. Equations (1) and (2) satisfy the assumption that the vertical lines become parabolic. The last term in eqn (1) arises from the deformation of pure bending. Equation (3) represents the assumption that planes parallel to the rigid plates remain planar.

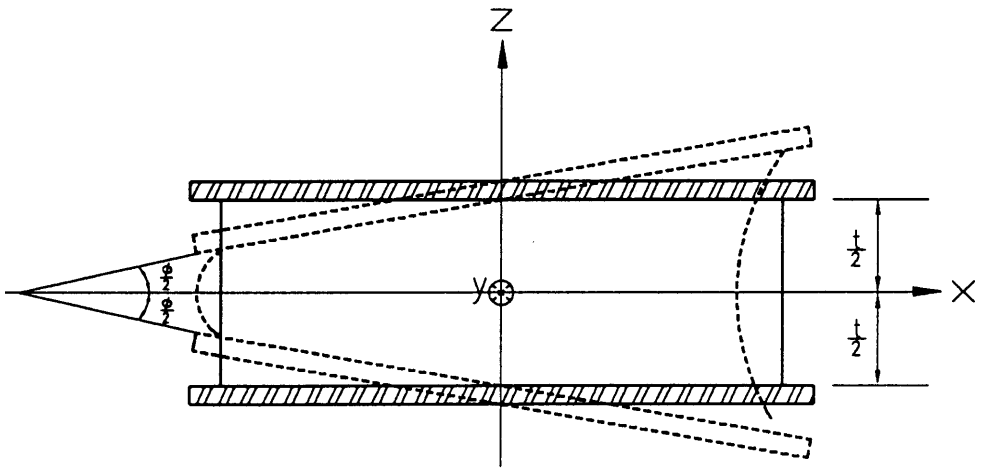


Fig. 2. Deformed shape of a tilted layer.

For an isotropic elastic material, the mean pressure $p$ has the following relation with displacements

$$p(x,y,z) = -\kappa(u_{,x}+v_{,y}+w_{,z}) \tag{4}$$

where $\kappa$ is the bulk modulus and the commas imply partial differentiation with respect to the indicated coordinates. The equilibrium equations in the $x$ and $y$ coordinate directions may be combined (Tsai and Lee, 1998) to become

$$(u_{,x}+v_{,y})_{,xx}+(u_{,x}+v_{,y})_{,yy}+(u_{,x}+v_{,y})_{,zz} = \frac{\lambda+\mu}{\mu\kappa}(p_{,xx}+p_{,yy}) \tag{5}$$

in which $\lambda$ and $\mu$ are Lamé's constants. Substituting the displacement assumptions in eqns (1)–(3) into eqns (4) and (5) and integrating the resulting equations through the thickness produces

$$\bar{u}_{,x}+\bar{v}_{,y} = -\frac{3}{2}\left(\frac{x}{\rho}+\frac{1}{\kappa}\bar{p}\right) \tag{6}$$

and

$$\frac{2}{3}[(\bar{u}_{,x}+\bar{v}_{,y})_{,xx}+(\bar{u}_{,x}+\bar{v}_{,y})_{,yy}]-\frac{8}{t^2}(\bar{u}_{,x}+\bar{v}_{,y}) = \frac{\lambda+\mu}{\mu\kappa}(\bar{p}_{,xx}+\bar{p}_{,yy}) \tag{7}$$

where $\bar{p}$ is the effective pressure defined as

$$\bar{p}(x,y) = \frac{1}{t}\int_{-t/2}^{t/2} p(x,y,z)\,\mathrm{d}z \tag{8}$$

The governing equation for the effective pressure is obtained by substituting eqn (6) into eqn (7),

$$\bar{p}_{,xx}+\bar{p}_{,yy}-2\alpha^2\bar{p} = 2\alpha^2\frac{\kappa}{\rho}x \tag{9}$$

in which $\alpha$ is defined as

$$\alpha = \sqrt{\frac{6\mu}{t^2(\lambda+2\mu)}} \tag{10}$$

Equation (9) is solved by satisfying the boundary conditions so that the stresses are free on the unbonded surfaces of the elastic layer. In the 'approximate pressure' solution, the differential equation is similar to eqn (9), but the coefficient $\alpha$ is different; the boundary conditions are assumed as $\bar{p}(x,y) = 0$ on the stress-free surfaces.

According to the elementary beam theory, the effective tilting stiffness of the layer is defined as

$$(EI)_{\mathrm{eff}} = \rho\int_A \bar{\sigma}_{zz}x\,\mathrm{d}x\,\mathrm{d}y \tag{11}$$

where the integration represents the total applied moment and $\bar{\sigma}_{zz}$ is the effective vertical stress defined as

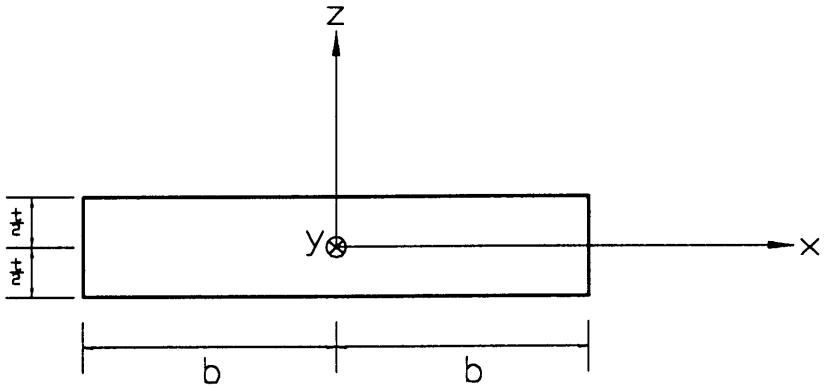


Fig. 3. Dimensions of an infinite-strip layer.

$$\bar{\sigma}_{zz} = \frac{1}{t}\int_{-t/2}^{t/2} \sigma_{zz}\,\mathrm{d}z \tag{12}$$

Using the following stress expression for the vertical stress,

$$\sigma_{zz} = -\frac{\lambda}{\kappa}p + 2\mu w_{,z} \tag{13}$$

the effective tilting stiffness becomes

$$(EI)_{\text{eff}} = 2\mu I_y - \frac{\rho\lambda}{\kappa}\int_A x\bar{p}(x,y)\,\mathrm{d}x\,\mathrm{d}y \tag{14}$$

where $I_y = \int_A x^2\,\mathrm{d}x\,\mathrm{d}y$ is the moment of inertia of the cross-section area about the $y$ axis.

## 3. Layer of infinite-strip shape

The infinite-strip layer shown in Fig. 3 has a width of $2b$ and a thickness of $t$. The corresponding shape factor is $S_i = b/t$. The moment of inertia for the unit length of strip is $I_i = 2b^3/3$. If the $y$ coordinate direction is attached to the infinite-long side, the displacement component $v$ vanishes and the layer is in plane-strain parallel to the $xz$ plane. The governing equation for the effective pressure in eqn (9) becomes

$$\bar{p}_{,xx} - \bar{\alpha}^2\bar{p} = \frac{1}{\rho}\bar{\alpha}^2\kappa x \tag{15}$$

in which $\bar{\alpha}$ satisfies the relation

$$\bar{\alpha}b = 2S_i\sqrt{\frac{3\mu}{\lambda+2\mu}} \tag{16}$$

The normal stress $\sigma_{xx}$ in the plane-strain state can be expressed (Tsai and Lee, 1998) as

$$\sigma_{xx} = -\frac{\lambda+2\mu}{\kappa}p - 2\mu w_{,z} \tag{17}$$

By substituting the displacement assumption in eqn (3) into the above equation and integrating the resulting equation through the thickness, the boundary condition at $x = b$, $\sigma_{xx} = 0$, yields

$$\bar{p}(b) = -\frac{b}{\rho}\left(\frac{2\mu\kappa}{\lambda+2\mu}\right) \tag{18}$$

Satisfying the above boundary condition, the function $\bar{p}(x)$ can be solved from eqn (15), as below

$$\bar{p}(x) = \kappa\frac{b}{\rho}\left[\frac{\lambda\sinh(\bar{\alpha}x)}{(\lambda+2\mu)\sinh(\bar{\alpha}b)} - \frac{x}{b}\right] \tag{19}$$

Substituting the above equation into eqn (14) yields

$$\frac{(EI)_{\text{eff}}}{I_i} = 2\mu+\lambda\left[1-\frac{\lambda}{\lambda+2\mu}\frac{3}{(\bar{\alpha}b)^2}\left(\frac{\bar{\alpha}b}{\tanh(\bar{\alpha}b)}-1\right)\right] \tag{20}$$

which is a multiple of Young's modulus $E$ and also a function of Poisson's ratio $v$ and shape factor $S_i$.

Figure 4 plots the variation of the tilting stiffness calculated from eqn (20) with respect to $v$ for $S_i = 2$ and $S_i = 20$. Also plotted in the figure is the finite element solution where the infinite-strip layer is modeled by eight-node isoparametric plane-strain elements. The figure shows that the tilting stiffness calculated by eqn (20) is extremely close to the finite element solution.

The formula derived by Lindley (1979b) for the tilting stiffness of an infinite-strip layer can be expressed as

$$\frac{(EI)_{\text{eff}}}{I_i} = \begin{cases} 2\mu+\lambda\left[1-\dfrac{\lambda}{\lambda+2\mu}\left(1-\dfrac{(\bar{\alpha}b)^2}{15}\dfrac{1+\dfrac{1}{210}(\bar{\alpha}b)^2}{1+\dfrac{1}{10}(\bar{\alpha}b)^2}\right)\right] & \text{for } \bar{\alpha}b \leqslant \sqrt{15} \\ 2\mu+\lambda\left[1-\dfrac{\lambda}{\lambda+2\mu}\left(\dfrac{2.656}{\bar{\alpha}b}+\dfrac{0.0536}{(\bar{\alpha}b)^2}-\dfrac{9.752}{(\bar{\alpha}b)^3}+\dfrac{11.25}{(\bar{\alpha}b)^4}\right)\right] & \text{for } \bar{\alpha}b > \sqrt{15} \end{cases} \tag{21}$$

This formula is similar to eqn (20) except for the function of $\bar{\alpha}b$ in the parentheses. Figure 4 shows that the curve of eqn (21) is almost the same as the curve of eqn (20). However, the expression in eqn (20) is more compact that eqn (21).

The 'approximate pressure' solution derived by Chalhoub and Kelly (1991) is

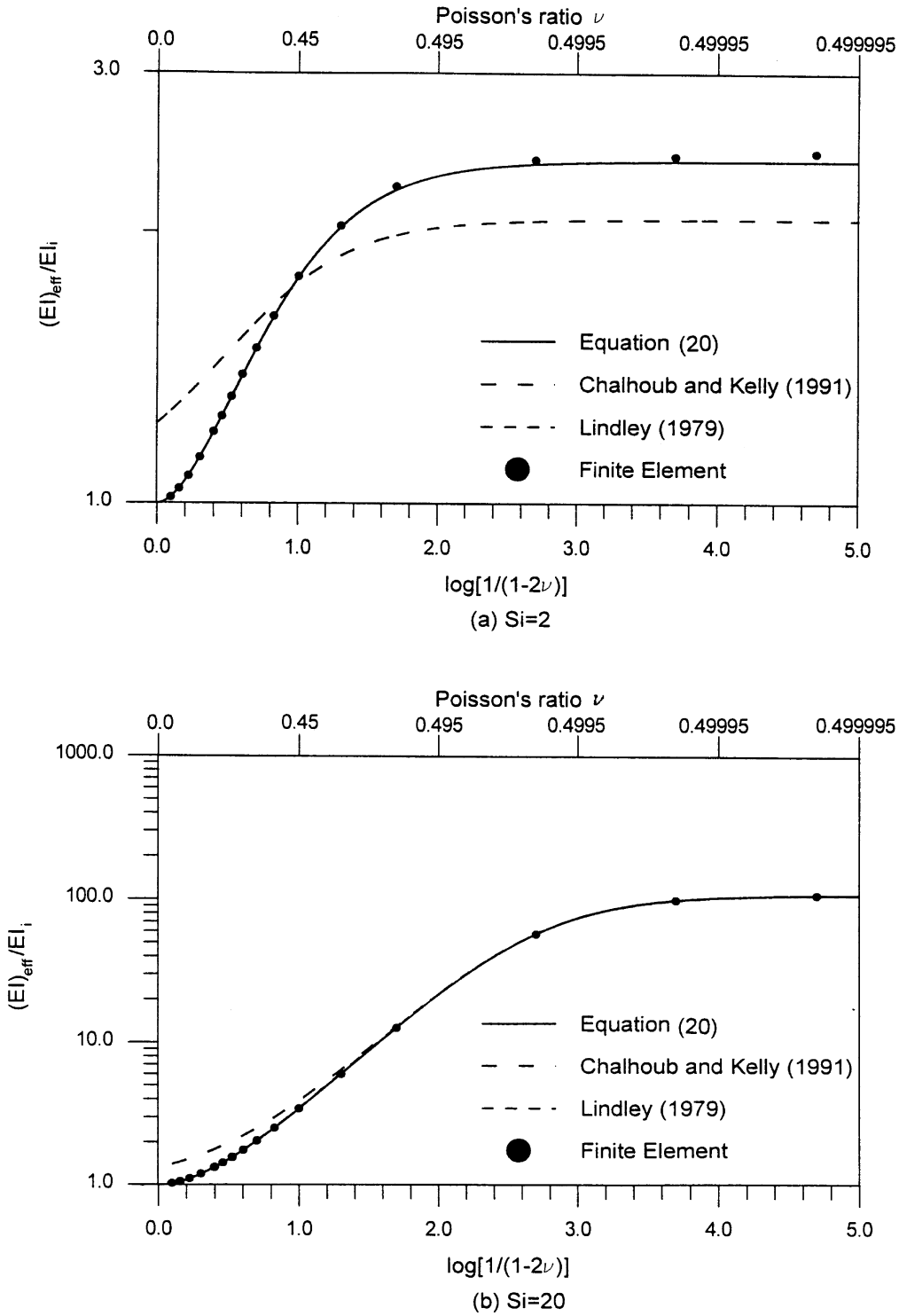


Fig. 4. Effective tilting stiffness of infinite-strip layer.

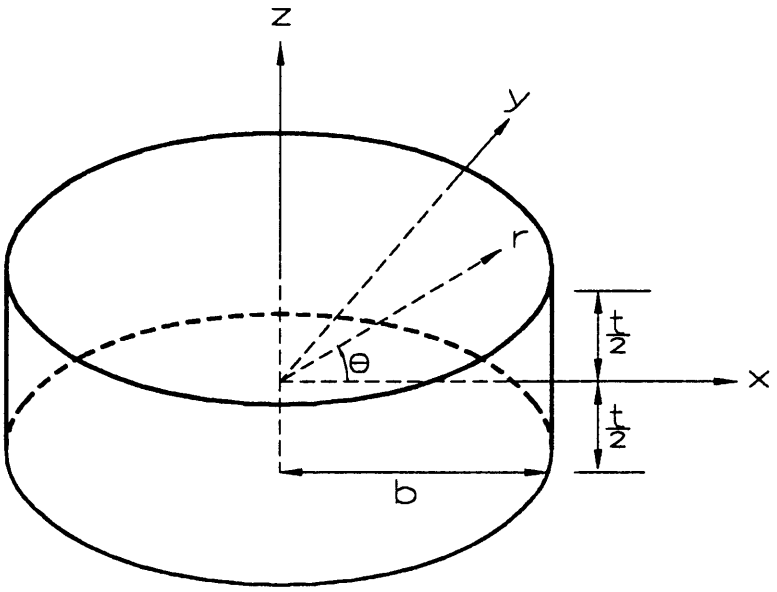


Fig. 5. Dimensions of a circular layer.

$$\frac{(EI)_{\text{eff}}}{I_i} = E+\kappa\left[1-\frac{3}{(\hat{\alpha}b)^2}\left(\frac{\hat{\alpha}b}{\tanh(\hat{\alpha}b)}-1\right)\right] \tag{22}$$

in which

$$\hat{\alpha}b = 2S_i\sqrt{\frac{3\mu}{\kappa}} \tag{23}$$

As shown in Fig. 4, the 'approximate pressure' solution is accurate only when the layer has high shape factor and the material has Poisson's ratio greater than 0.45.

If the layer's material is nearly incompressible, $\bar{\alpha}b$ becomes infinitesimal. By applying the following approximation

$$\frac{\bar{\alpha}b}{\tanh(\bar{\alpha}b)} \approx 1+\frac{1}{3}(\bar{\alpha}b)^2-\frac{1}{45}(\bar{\alpha}b)^4 \tag{24}$$

in eqn (20), the effective tilting stiffness of incompressible material for the infinite-strip layer is obtained as

$$\frac{(EI)_{\text{eff}}}{I_i} = 4\mu\left(1+\frac{1}{5}S_i^2\right) \tag{25}$$

## 4. Layer of circular shape

The circular layer shown in Fig. 5 has a radius of $b$ and a thickness of $t$. The corresponding shape factor is $S_c = b/(2t)$ and the moment of inertia for the circular area is $I_c = \pi b^4/4$. A cylindrical

polar coordinate system $(r, \theta, z)$ is established with the origin at the center of the layer. The rigid plates on the top and bottom of the layer rotate about the axis in the direction of $\theta = \pi/2$. Denote $u$, $v$ and $w$ as the displacements along the $r$, $\theta$ and $z$ directions, respectively. Applying coordinate transformation, the displacement assumptions in eqns (1)–(3) become

$$u(r,\theta,z) = \bar{u}(r,\theta)\left(1-\frac{4z^2}{t^2}\right)-\frac{1}{2\rho}z^2\cos\theta \tag{26}$$

$$v(r,\theta,z) = \bar{v}(r,\theta)\left(1-\frac{4z^2}{t^2}\right)+\frac{1}{2\rho}z^2\sin\theta \tag{27}$$

$$w(r,\theta,z) = \frac{1}{\rho}rz\cos\theta \tag{28}$$

The expression of the mean pressure in the cylindrical coordinate system is

$$p(r,\theta,z) = -\kappa\left(u_{,r}+\frac{u}{r}+\frac{v_{,\theta}}{r}+w_{,z}\right) \tag{29}$$

The equilibrium equation in the $r$ direction is

$$2\left(u_{,rr}+\frac{u_{,r}}{r}-\frac{u}{r^2}\right)+\frac{1}{r^2}u_{,\theta\theta}+u_{,zz}+\frac{1}{r}\left(v_{,r\theta}-\frac{3}{r}v_{,\theta}\right)+w_{,rz} = \frac{\lambda}{\mu\kappa}p_{,r} \tag{30}$$

Substituting eqns (26)–(28) into eqns (29) and (30) and integrating the resulting equations through the thickness leads to

$$\bar{u}_{,r}+\frac{1}{r}\bar{v}_{,\theta}+\frac{1}{r}\bar{u} = -\frac{3}{2\rho}r\cos\theta-\frac{3}{2\kappa}\bar{p} \tag{31}$$

and

$$\bar{u}_{,rr}+\frac{1}{r}\bar{u}_{,r}-\left(\frac{6}{t^2}+\frac{1}{r^2}\right)\bar{u}+\frac{1}{2r^2}\bar{u}_{,\theta\theta}+\frac{1}{2r}\bar{v}_{,r\theta}-\frac{3}{2r^2}\bar{v}_{,\theta} = \frac{3\lambda}{4\mu\kappa}\bar{p}_{,r} \tag{32}$$

Differentiating eqn (31) with respect to $r$ and subtracting the result from eqn (32) yields

$$\frac{6}{t^2}\bar{u}-\frac{1}{2r^2}\bar{u}_{,\theta\theta}+\frac{1}{2r}\bar{v}_{,r\theta}+\frac{1}{2r^2}\bar{v}_{,\theta} = -\frac{3(\lambda+2\mu)}{4\mu\kappa}\bar{p}_{,r}-\frac{3}{2\rho}\cos\theta \tag{33}$$

After taking coordinate transformation, the governing equation for the effective pressure in eqn (9) becomes

$$\bar{p}_{,rr}+\frac{1}{r}\bar{p}_{,r}+\frac{1}{r^2}\bar{p}_{,\theta\theta}-\bar{\alpha}^2\bar{p} = \bar{\alpha}^2\frac{\kappa}{\rho}r\cos\theta \tag{34}$$

where $\bar{\alpha}$ satisfies the relation

$$\bar{\alpha}b = 4S_c\sqrt{\frac{3\mu}{\lambda+2\mu}} \tag{35}$$

The effective pressure is symmetric to the $r$ axis at $\theta = 0$ and antisymmetric to the $r$ axis at $\theta = \pi/2$, i.e.

$$\bar{p}(r,\theta) = \bar{p}(r,-\theta) = -\bar{p}(r,\pi-\theta) \tag{36}$$

To satisfy the above conditions, the solution of eqn (34) has the following expression

$$\bar{p}(r,\theta) = -\frac{\kappa}{\rho}r\cos\theta + \sum_{n=1}^{\infty} A_n I_{2n-1}(\bar{\alpha}r)\cos(2n-1)\theta \tag{37}$$

where $I_n$ is the modified Bessel function of the first kind of order $n$ and $A_n$ is the constants to be determined. By taking coordinate transformation and applying eqn (37), the effective tilting stiffness in eqn (14) becomes

$$(EI)_{\text{eff}} = I_c\left[\lambda+2\mu - A_1\frac{4\lambda\rho}{\kappa\bar{\alpha}b^2}I_2(\bar{\alpha}b)\right] \tag{38}$$

which indicates that, to obtain the tilting stiffness, $A_1$ is the only constant necessary to be solved.

The displacement $u$ is symmetric and $v$ is antisymmetric with respect to the $r$ axis at $\theta = 0$. Since the effective pressure $\bar{p}$ in eqn (37) is a cosine series, eqn (31) implies that $\bar{u}$ can be expressed as a cosine series

$$\bar{u}(r,\theta) = \sum_{n=1}^{\infty} \bar{u}^{(n)}(r)\cos(2n-1)\theta \tag{39}$$

and $\bar{v}$ as a sine series

$$\bar{v}(r,\theta) = \sum_{n=1}^{\infty} \bar{v}^{(n)}(r)\sin(2n-1)\theta \tag{40}$$

where $\bar{u}^{(n)}$ and $\bar{v}^{(n)}$ are the amplitudes of the $n$th term in $\bar{u}$ and $\bar{v}$, respectively. Substituting eqns (37), (39) and (40) into eqn (31) yields

$$\bar{u}^{(1)}_{,r} + \frac{1}{r}\bar{v}^{(1)} + \frac{1}{r}\bar{u}^{(1)} = -\frac{3}{2\kappa}A_1 I_1(\bar{\alpha}r) \tag{41}$$

Similarly, eqn (33) gives

$$-\left(\frac{1}{2r^2}+\frac{6}{t^2}\right)\bar{u}^{(1)} - \frac{1}{2r}\left(\bar{v}^{(1)}_{,r} + \frac{1}{r}\bar{v}^{(1)}\right) = \frac{3(\lambda+2\mu)}{4\mu\kappa}A_1\left[\bar{\alpha}I_0(\bar{\alpha}r) - \frac{1}{r}I_1(\bar{\alpha}r)\right] - \frac{3\lambda}{4\rho\mu} \tag{42}$$

The boundary conditions are $r = b$ give

$$\sigma_{rr} = -\frac{\lambda}{\kappa}p + 2\mu u_{,r} = 0 \tag{43}$$

and

$$\tau_{r\theta} = \mu\left(\frac{u_{,\theta}}{r} + v_{,r} - \frac{v}{r}\right) = 0 \tag{44}$$

Substituted by eqns (26) and (27) and integrated through the thickness, eqns (43) and (44) become

$$\bar{u}_{,r}(b,\theta) = \frac{3\lambda}{4\mu\kappa}\bar{p}(b,\theta) \tag{45}$$

and

$$\bar{v}_{,r}(b,\theta) = \frac{1}{b}[\bar{v}(b,\theta) - \bar{u}_{,\theta}(b,\theta)] \tag{46}$$

Substituting eqns (37), (39) and (40) into the above two equations yields

$$\bar{u}^{(1)}_{,r}(b) = \frac{3\lambda}{4\mu\kappa}A_1 I_1(\bar{\alpha}b) - \frac{3\lambda b}{4\mu\rho} \tag{47}$$

and

$$\bar{v}^{(1)}_{,r}(b) = \frac{1}{b}[\bar{v}^{(1)}(b) + \bar{u}^{(1)}(b)] \tag{48}$$

Since the rigid plates rotate about the $r$ axis at $\theta = \pi/2$, it is reasonable to assume $\bar{v}(b, \pm\pi/2) = 0$ which indicates

$$\bar{v}^{(1)}(b) = 0 \tag{49}$$

The expression of $\bar{u}^{(1)}(b)$ can be derived by substituting eqns (47) and (49) into eqn (41) for $r = b$. Then, by substituting $\bar{u}^{(1)}(b)$, $\bar{v}^{(1)}(b)$ and $\bar{v}^{(1)}_{,r}(b)$ into eqn (42) for $r = b$, $A_1$ is solved as

$$A_1 = \frac{24b\kappa\lambda S_c^2}{\rho(\lambda+2\mu)[2(1+12S_c^2)I_1(\bar{\alpha}b) - \bar{\alpha}bI_0(\bar{\alpha}b)]} \tag{50}$$

Substituting the above equation into eqn (38) leads to

$$\frac{(EI)_{\text{eff}}}{I_c} = 2\mu + \lambda\left[1 - \left(\frac{2\lambda}{\mu}\right)\frac{\bar{\alpha}bI_0(\bar{\alpha}b) - 2I_1(\bar{\alpha}b)}{2(1+12S_c^2)I_1(\bar{\alpha}b) - \bar{\alpha}bI_0(\bar{\alpha}b)}\right] \tag{51}$$

The variations of tilting stiffness with respect to $v$, as calculated from eqn (51), are compared with the finite element solution and the 'approximate pressure' solution (Chalhoub and Kelly, 1990) in Fig. 6 for $S_c = 2$ and $S_c = 20$. In the finite element analysis, the circular layer is modeled by eight-node solid elements with incompatible bending modes. The figure shows that the tilting stiffness calculated by eqn (51) is extremely close to the finite element solution, whereas the 'approximate pressure' solution is accurate only when the layer has high shape factor and Poisson's ratio greater than 0.45.

When the layer's material is nearly incompressible, $\bar{\alpha}b$ tends to infinitesimal and the following function of $\bar{\alpha}b$ in eqn (51) may be approximated by

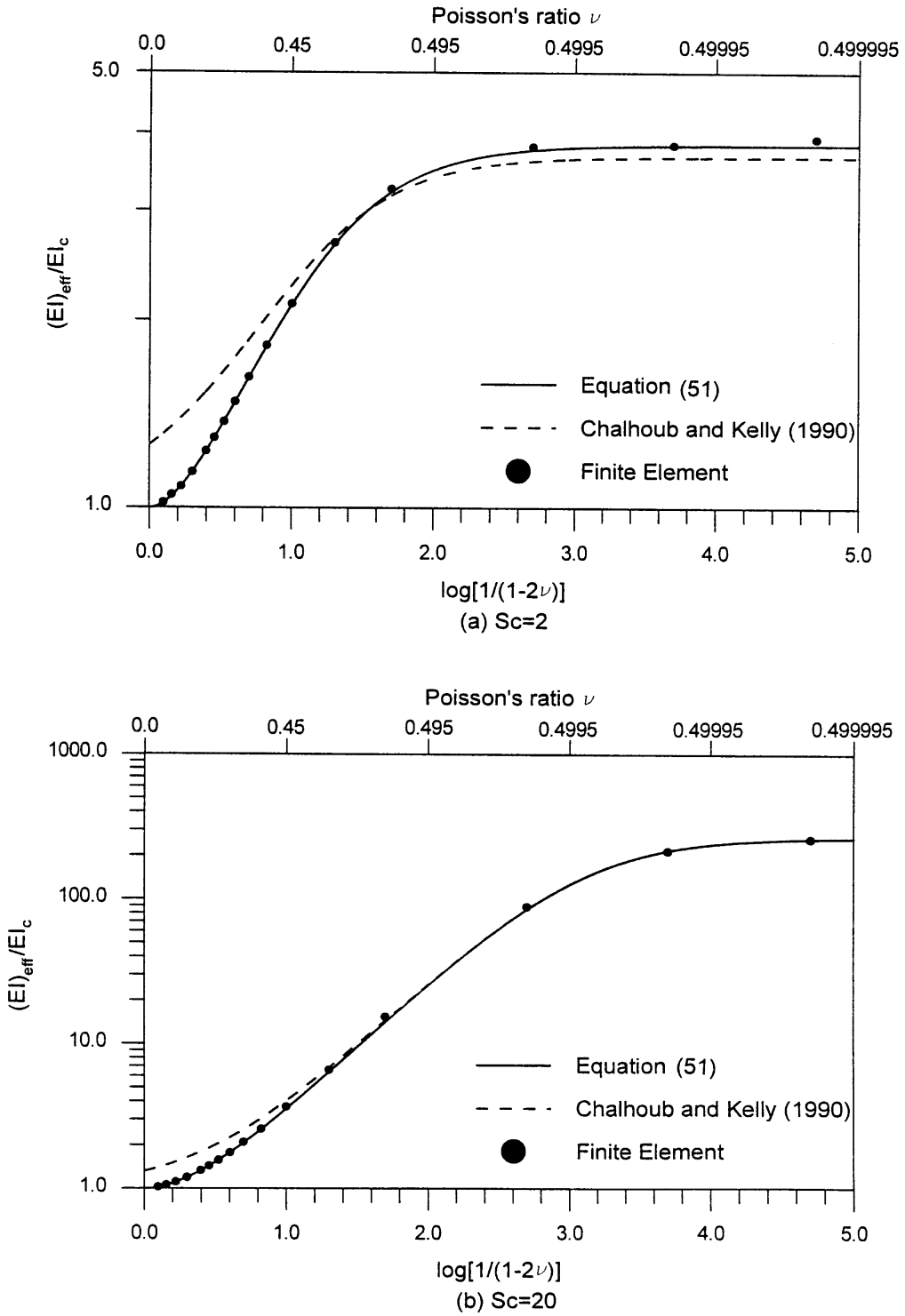


Fig. 6. Effective tilting stiffness of circular layer.

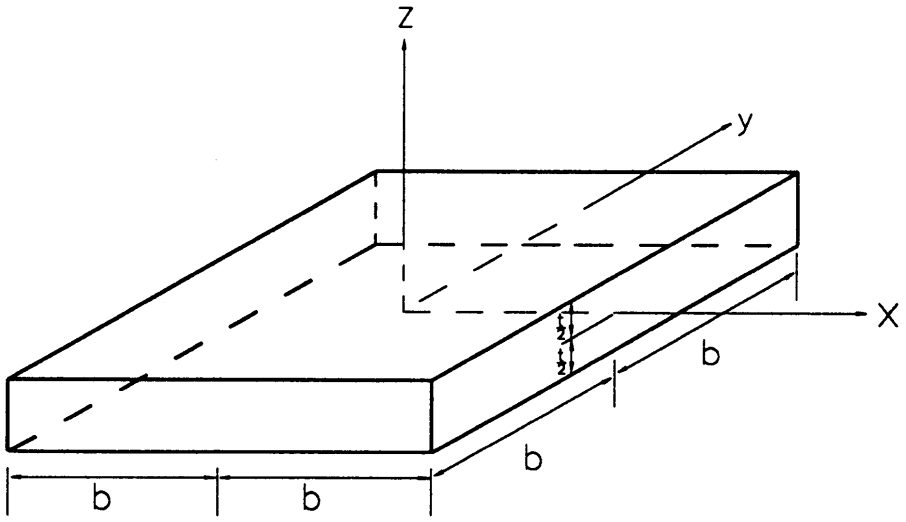


Fig. 7. Dimensions of a square layer.

$$\frac{\bar{\alpha}bI_0(\bar{\alpha}b)}{2I_1(\bar{\alpha}b)} \approx 1+\frac{1}{8}(\bar{\alpha}b)^2-\frac{1}{192}(\bar{\alpha}b)^4 \tag{52}$$

Consequently, the effective tilting of incompressible material for the circular shape is

$$\frac{(EI)_{\text{eff}}}{I_c} = \mu(3.5+2S_c^2) \tag{53}$$

## 5. Layer of square shape

The elastic layer of square shape shown in Fig. 7 has a side length of $2b$ and a thickness of $t$. The corresponding shape factor is $S_s = b/(2t)$ and the moment of inertia for the square shape is $I_s = 4b^4/3$. The boundary conditions at $x = b$ give

$$\sigma_{xx} = -\frac{\lambda}{\kappa}p+2\mu u_{,x} = 0 \tag{54}$$

and

$$\tau_{xy} = \mu(u_{,y}+v_{,x}) = 0 \tag{55}$$

Substituting eqns (1) and (2) into the above equations and integrating the results through the depth yields

$$\bar{p}(b,y)=\frac{4\mu\kappa}{3\lambda}\bar{u}_{,x}(b,y) \tag{56}$$

and

$$\bar{u}_{,y}(b,y)+\bar{v}_{,x}(b,y)=0 \tag{57}$$

Similarly, at $y=b$, the boundary conditions

$$\sigma_{yy}=-\frac{\lambda}{\kappa}p+2\mu v_{,y}=0 \tag{58}$$

and $\tau_{yx}=0$ leads to

$$\bar{p}(x,b)=\frac{4\mu\kappa}{3\lambda}\bar{v}_{,y}(x,b) \tag{59}$$

and

$$\bar{u}_{,y}(x,b)+\bar{v}_{,x}(x,b)=0 \tag{60}$$

The distribution of the effective pressure is derived by solving the partial differential equation in eqn (9). The particular solution of eqn (9), $\bar{p}_{\mathrm{p}}$, is

$$\bar{p}_{\mathrm{p}}=-\frac{\kappa}{\rho}x \tag{61}$$

while the complementary solution of eqn (9), $\bar{p}_{\mathrm{c}}$, is solved by the method of separation of variables. By defining $\bar{p}_{\mathrm{c}}(x,y)=\bar{X}(x)\bar{Y}(y)$, the functions $\bar{X}$ and $\bar{Y}$ must satisfy the following relation

$$\frac{\bar{X}''-\alpha^2\bar{X}}{\bar{X}}=-\frac{\bar{Y}''-\alpha^2\bar{Y}}{\bar{Y}}=C \tag{62}$$

where $C$ is a constant. If $\bar{p}_0$, $\bar{p}_+$ and $\bar{p}_-$ are denoted as the solution of $\bar{p}_{\mathrm{c}}$ when $C=0$, $C>0$ and $C<0$, respectively, the complete solution of $\bar{p}$ becomes

$$\bar{p}(x,y)=\bar{p}_{\mathrm{p}}(x,y)+\bar{p}_0(x,y)+\bar{p}_+(x,y)+\bar{p}_-(x,y) \tag{63}$$

When the rigid bonding plates rotate about the $y$ axis, the effective pressure acting on the square layer is symmetric about the $x$ axis and anti-symmetric about the $y$ axis, i.e.

$$\bar{p}(x,y)=\bar{p}(x,-y)=-\bar{p}(-x,y) \tag{64}$$

By substituting eqn (56) at $y=b$ and eqn (59) at $x=b$ into eqn (6), the effective pressure on the corner is found as

$$\bar{p}(b,b)=-\frac{b}{\rho}\left(\frac{\mu\kappa}{\lambda+\mu}\right) \tag{65}$$

If the following conditions on the corners are set

$$\bar{p}_+(b,b) = \bar{p}_-(b,b) = 0 \tag{66}$$

eqns (65) and (61) imply

$$\bar{p}_0(b,b) = \frac{b}{\rho}\left(\frac{\lambda\kappa}{\lambda+\mu}\right) \tag{67}$$

The function $\bar{p}_0(x,y)$ can be solved by satisfying the conditions in eqns (64) and (67)

$$\bar{p}_0(x,y) = \frac{b}{\rho}\left(\frac{\lambda\kappa}{\lambda+\mu}\right)\frac{\sinh(\alpha x)\cosh(\alpha y)}{\sinh(\alpha b)\cosh(\alpha b)} \tag{68}$$

To satisfy eqns (64) and (66), $\bar{p}_+$ has the expression

$$\bar{p}_+(x,y) = \sum_{n=1}^{\infty} A_n \sinh(\beta_n x)\cos(\gamma_n y) \tag{69}$$

with

$$\beta_n = \sqrt{2\alpha^2+\gamma_n^2}; \quad \gamma_n = \frac{(2n-1)\pi}{2b} \quad n = 1,2,,\ldots,\infty \tag{70}$$

and $\bar{p}_-$ has the expression

$$\bar{p}_-(x,y) = \sum_{n=1}^{\infty} \bar{A}_n \sin(\bar{\gamma}_n x)\cosh(\bar{\beta}_n y) \tag{71}$$

with

$$\bar{\beta}_n = \sqrt{2\alpha^2+\bar{\gamma}_n^2}; \quad \bar{\gamma}_n = \frac{n\pi}{b} \quad n = 1,2,,\ldots,\infty \tag{72}$$

where $A_n$ and $\bar{A}_n$ are the constants to be determined.

Consequently, the effective pressure defined in eqn (63) has the following expression

$$\bar{p}(x,y) = \kappa\frac{b}{\rho}\left[-\frac{x}{b} + \frac{\lambda}{\lambda+\mu}\frac{\sinh(\alpha x)\cosh(\alpha y)}{\sinh(\alpha b)\cosh(\alpha b)}\right] + \sum_{n=1}^{\infty}\left[A_n \sinh(\beta_n x)\cos(\gamma_n y) + \bar{A}_n \sin(\bar{\gamma}_n x)\cosh(\bar{\beta}_n y)\right] \tag{73}$$

Substituting the above equation into eqn (14) produces

$$\frac{(EI)_{\text{eff}}}{I_s} = 2\mu+\lambda-\frac{3\lambda^2}{\lambda+\mu}\left[\frac{\alpha b-\tanh(\alpha b)}{(\alpha b)^3}\right]+\frac{3\lambda}{\kappa}\sum_{n=1}^{\infty}\left[\bar{a}_n - a_n\left(1-\frac{\tanh(\beta_n b)}{\beta_n b}\right)\right] \tag{74}$$

where $a_n$ is a multiple of $A_n$ defined as

$$a_n = \frac{\rho}{b} A_n \frac{\cosh(\beta_n b)\sin(\gamma_n b)}{(\beta_n b)(\gamma_n b)} \tag{75}$$

and $\bar{a}_n$ is a multiple of $\bar{A}_n$ defined as

$$\bar{a}_n = \frac{\rho}{b} \bar{A}_n \frac{\sinh(\bar{\beta}_n b)\cos(\bar{\gamma}_n b)}{(\bar{\beta}_n b)(\bar{\gamma}_n b)} \tag{76}$$

To find $a_n$ and $\bar{a}_n$, substitute the expression of $\bar{p}(b, y)$ as obtained from eqn (73) into eqn (56) to find $\bar{u}_{,x}(b, y)$. Then, substituting $\bar{u}_{,x}(b, y)$ and $\bar{p}(b, y)$ into eqn (6) with $x = b$ produces

$$\bar{v}_{,y}(b, y) = \frac{3b\lambda}{4\rho\mu}\left[1 - \left(\frac{\lambda+2\mu}{\lambda+\mu}\right)\frac{\cosh(\alpha y)}{\cosh(\alpha b)}\right] - \frac{3(\lambda+2\mu)}{4\mu\kappa}\sum_{n=1}^{\infty} A_n \sinh(\beta_n b)\cos(\gamma_n y) \tag{77}$$

Also, substituting the expressions of $\bar{p}(x, b)$ as obtained from eqn (73) into eqn (59) produces

$$\bar{v}_{,y}(x, b) = \frac{3b\lambda}{4\rho\mu}\left[-\frac{x}{b} + \left(\frac{\lambda}{\lambda+\mu}\right)\frac{\sinh(\alpha x)}{\sinh(\alpha b)}\right] + \frac{3\lambda}{4\mu\kappa}\sum_{n=1}^{\infty} \bar{A}_n \cosh(\bar{\beta}_n b)\sin(\bar{\gamma}_n x) \tag{78}$$

Equations (77) and (78) indicate

$$\begin{aligned}\bar{v}_{,y}(x, y) = \frac{3b\lambda}{4\rho\mu}&\left[-\frac{x}{b} + 2\frac{\sinh(\alpha x)}{\sinh(\alpha b)} - \left(\frac{\lambda+2\mu}{\lambda+\mu}\right)\frac{\sinh(\alpha x)\cosh(\alpha y)}{\sinh(\alpha b)\cosh(\alpha b)}\right] \\ &- \frac{3(\lambda+2\mu)}{4\kappa\mu}\sum_{n=1}^{\infty} A_n \sinh(\beta_n x)\cos(\gamma_n y) + \frac{3\lambda}{4\mu\kappa}\sum_{n=1}^{\infty} \bar{A}_n \cosh(\bar{\beta}_n y)\sin(\bar{\gamma}_n x)\end{aligned} \tag{79}$$

The expressions for $\bar{v}(x, y)$ can be derived by integrating the above equation with respect to $y$ and applying the condition $\bar{v}(x, 0) = 0$.

By substituting the derived $\bar{v}(x, y)$ and $\bar{p}(x, y)$ in eqn (73) into eqn (6), the expression for $\bar{u}_{,x}(x, y)$ is derived and then is integrated with respect to $x$ to obtain

$$\begin{aligned}\bar{u}(x, y) = \frac{3b}{4\mu\rho}&\left[\frac{x^2}{2b} - \frac{2\cosh(\alpha x)}{\alpha\sinh(\alpha b)} + \left(\frac{\lambda}{\lambda+\mu}\right)\frac{\cosh(\alpha x)\cosh(\alpha y)}{\alpha\sinh(\alpha b)\cosh(\alpha b)}\right] \\ &+ \frac{3\lambda}{4\mu\kappa}\sum_{n=1}^{\infty}\left[\frac{A_n}{\beta_n}\cosh(\beta_n x)\cos(\gamma_n y) + \left(\frac{\lambda+2\mu}{\lambda}\right)\frac{\bar{A}_n}{\bar{\gamma}_n}\cos(\bar{\gamma}_n x)\cosh(\bar{\beta}_n y)\right] + f(y)\end{aligned} \tag{80}$$

where $f(y)$ represents a function of $y$, which can be determined by assuming that the layer's edge at $x = b$ remains straight after deformation, i.e., $\bar{u}(b, y)$ is a constant value independent of $y$.

Substituting the derived expressions of $\bar{u}(x, y)$ and $\bar{v}(x, y)$ into eqn (57) produces

$$\begin{aligned}\frac{\lambda+2\mu}{\kappa}\sum_{n=1}^{\infty}\left[A_n\frac{\beta_n}{\gamma_n}\cosh(\beta_n b)\sin(\gamma_n y)\right] - \frac{\lambda}{\kappa}\sum_{n=1}^{\infty}\left[\bar{A}_n\frac{\bar{\gamma}_n}{\bar{\beta}_n}\sinh(\bar{\beta}_n y)\cos(\bar{\gamma}_n b)\right] \\ = \frac{\lambda b}{\rho}\left[-\frac{y}{b} + \frac{2\alpha y}{\tanh(\alpha b)} - \left(\frac{\lambda+2\mu}{\lambda+\mu}\right)\frac{\sinh(\alpha y)}{\sinh(\alpha b)}\right]\end{aligned} \tag{81}$$

Multiplying both sides of the above equation by $\sin(\gamma_m y)$ and integrating from $y = -b$ to $y = b$ gives

$$a_m = \sum_{n=1}^{\infty} F_{mn}\bar{a}_n + f_m \quad m = 1, 2, \ldots, \infty \tag{82}$$

in which

$$F_{mn} = \left(\frac{2\lambda}{\lambda+2\mu}\right)\frac{(\bar{\gamma}_n b)^2(\bar{\beta}_n b)}{(\beta_m b)^2[(\bar{\beta}_n b)^2 + (\gamma_m b)^2]\tanh(\bar{\beta}_n b)} \tag{83}$$

and

$$f_m = \left(\frac{2\kappa\lambda}{\lambda+2\mu}\right)\left[\frac{\alpha b}{\tanh(\alpha b)}\right]\frac{1}{(\beta_m b)^2(\gamma_m b)^2}\left[1 - \frac{\tanh(\alpha b)}{\alpha b} + \frac{1}{1+\left(\frac{\alpha b}{\gamma_m b}\right)^2}\left(\left(\frac{\alpha b}{\gamma_m b}\right)^2 - \frac{\mu}{\lambda+\mu}\right)\right] \tag{84}$$

Similarly, substituting the derived expressions of $\bar{u}(x, y)$ and $\bar{v}(x, y)$ into eqn (60) produces

$$\begin{aligned}
&\sum_{n=1}^{\infty} A_n \sin(\gamma_n b)\left[\frac{\gamma_n}{\beta_n}\cosh(\beta_n b) - \left(\frac{\gamma_n}{\beta_n} + \frac{\lambda+2\mu}{\lambda}\frac{\beta_n}{\gamma_n}\right)\cosh(\beta_n x)\right] \\
&\quad - \sum_{n=1}^{\infty} \bar{A}_n \sinh(\bar{\beta}_n b)\left[\frac{\lambda+2\mu}{\lambda}\frac{\bar{\beta}_n}{\bar{\gamma}_n}\cos(\bar{\gamma}_n b) - \left(\frac{\bar{\gamma}_n}{\bar{\beta}_n} + \frac{\lambda+2\mu}{\lambda}\frac{\bar{\beta}_n}{\bar{\gamma}_n}\right)\cos(\bar{\gamma}_n x)\right] \\
&= \frac{b}{\rho\kappa}\left[\frac{2\mu}{\lambda+\mu}\frac{\cosh(\alpha x)}{\cosh(\alpha b)} - 2\alpha b\frac{\cosh(\alpha x)}{\sinh(\alpha b)} + \frac{2\lambda+\mu}{\lambda+\mu}\right]
\end{aligned} \tag{85}$$

Multiplying both sides of the above equation by $\cos(\bar{\gamma}_m x)$ and integrating from $x = -b$ to $x = b$ gives

$$\bar{a}_m = \sum_{n=1}^{\infty} G_{mn} a_n + g_m \quad m = 1, 2, \ldots, \infty \tag{86}$$

in which

$$G_{mn} = \frac{2}{(\beta_n b)^2 + (\bar{\gamma}_m b)^2}\left[\frac{(\gamma_n b)^2 + \left(1 + \frac{2\mu}{\lambda}\right)(\beta_n b)^2}{(\bar{\gamma}_m b)^2 + \left(1 + \frac{2\mu}{\lambda}\right)(\bar{\beta}_m b)^2}\right]\frac{\beta_n b}{\tanh(\beta_n b)} \tag{87}$$

and

$$g_m = \frac{-4\kappa}{(\bar{\gamma}_m b)^2 + \left(1+\frac{2\mu}{\lambda}\right)(\bar{\beta}_m b)^2}\left[\frac{(\alpha b)^2}{(\bar{\gamma}_m b)^2+(\alpha b)^2}\right]\left[1-\frac{\mu}{\lambda+\mu}\frac{\tanh(\alpha b)}{\alpha b}\right] \tag{88}$$

Approximated values of $a_n$ and $\bar{a}_n$ may be solved from eqns (82) and (86) if a finite upper bound of $m$ and $n$, say $k$, replaces the infinity in these equations. Denote $\mathbf{a}$ and $\bar{\mathbf{a}}$ be the vectors formed by $a_n$ and $\bar{a}_n$, respectively, of the first $k$ terms. Equations (82) and (86) can be replaced by matrix forms

$$\mathbf{a} = \mathbf{F}\bar{\mathbf{a}} + \mathbf{f} \tag{89}$$

$$\bar{\mathbf{a}} = \mathbf{G}\mathbf{a} + \mathbf{g} \tag{90}$$

where $\mathbf{F}$ and $\mathbf{G}$ are the matrices of $k \times k$ in which the elements $F_{mn}$ and $G_{mn}$ are defined in eqns (83) and (87), respectively; $\mathbf{f}$ and $\mathbf{g}$ are the $k$ dimensional vectors in which the elements $f_m$ and $g_m$ are defined in eqns (84) and (88), respectively. From eqns (89) and (90), $\mathbf{a}$ and $\bar{\mathbf{a}}$ are solved as

$$\mathbf{a} = (\mathbf{I}-\mathbf{F}\mathbf{G})^{-1}(\mathbf{F}\mathbf{g}+\mathbf{f}) \tag{91}$$

and

$$\bar{\mathbf{a}} = \mathbf{G}(\mathbf{I}-\mathbf{F}\mathbf{G})^{-1}(\mathbf{F}\mathbf{g}+\mathbf{f})+\mathbf{g} \tag{92}$$

where $\mathbf{I}$ is the unit matrix of $k \times k$.

According to eqn (10),

$$\alpha b = 2S_s\sqrt{\frac{6\mu}{\lambda+2\mu}} \tag{93}$$

Therefore, the ratio $(EI)_{\text{eff}}/I_s$ in eqn (74) is a multiple of Young's modulus $E$ and also a function of Poisson's ratio $v$ and shape factor $S_s$. Denote $(EI)_{\text{eff}}^{(k)}$ as the value of $(EI)_{\text{eff}}$ in eqn (74) including the first $k$ terms of $a_n$ and $\bar{a}_n$ solved from eqns (91) and (92). The ratios $(EI)_{\text{eff}}^{(1)}/(EI)_{\text{eff}}^{(50)}$ and $(EI)_{\text{eff}}^{(2)}/(EI)_{\text{eff}}^{(50)}$ are plotted in Fig. 8 for the varied $v$ and $S_s$. This figure shows that the difference ratio between $(EI)_{\text{eff}}^{(2)}$ and $(EI)_{\text{eff}}^{(50)}$ is close to 0.01 and the difference ratio between $(EI)_{\text{eff}}^{(1)}$ and $(EI)_{\text{eff}}^{(50)}$ is smaller than 0.05, which indicates the convergence of and $(EI)_{\text{eff}}^{(k)}$ is very fast and we can employ only the first terms of $a_n$ and $\bar{a}_n$ to approximate $(EI)_{\text{eff}}$ for an error smaller than five percent. The explicit form of $(EI)_{\text{eff}}^{(1)}$ is derived as

$$\frac{(EI)_{\text{eff}}^{(1)}}{I_s} = 2\mu+\lambda-\frac{3\lambda^2}{\lambda+\mu}\left[\frac{\alpha b-\tanh(\alpha b)}{(\alpha b)^3}\right]+\frac{3\lambda}{\kappa}\left[\frac{G_{11}f_1+g_1}{1-F_{11}G_{11}}-\left(1-\frac{\tanh(\beta_1 b)}{\beta_1 b}\right)\frac{F_{11}g_1+f_1}{1-F_{11}G_{11}}\right] \tag{94}$$

The values of tilting stiffness calculated from eqn (94) are compared with the finite element solution and the 'approximate pressure' solution (Koh and Kelly, 1987) in Fig. 9 for $S_s = 2$ and $S_s = 20$. In the finite element analysis, the square layer is modeled by eight-node solid elements with incompatible bending modes. The figure reveals that the tilting stiffness calculated from eqn

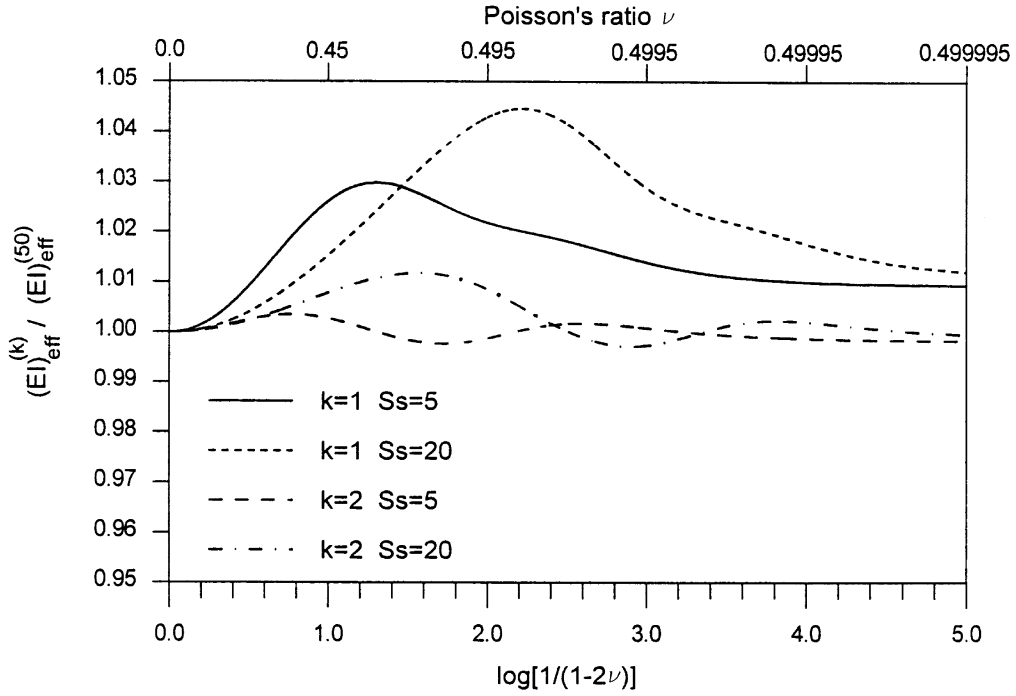


Fig. 8. Convergence of solution to the tilting stiffness of a square layer.

(94) is extremely close to the finite element solution and there are some deviations in the 'approximate pressure' solution.

When the layer's material is nearly incompressible, $\alpha b$ becomes infinitesimal. Applying the following approximation

$$\frac{\tanh(\alpha b)}{\alpha b} \approx 1 - \frac{1}{3}(\alpha b)^2 + \frac{2}{15}(\alpha b)^4 \tag{95}$$

in eqn (94), the tilting stiffness of incompressible material for the square shape can be solved as

$$\frac{(EI)^{(1)}_{\text{eff}}}{I_s} = 3\mu(1.133 + 0.7613 S_s^2) \tag{96}$$

In the first 50 terms of $a_n$ and $\bar{a}_n$ are considered in eqn (74), formula for the tilting stiffness of an incompressible layer is

$$\frac{(EI)^{(50)}_{\text{eff}}}{I_s} = 3\mu(1 + 0.7404 S_s^2) \tag{97}$$

which is close to the previously published results (Gent and Meinecke, 1970; Kelly, 1993).

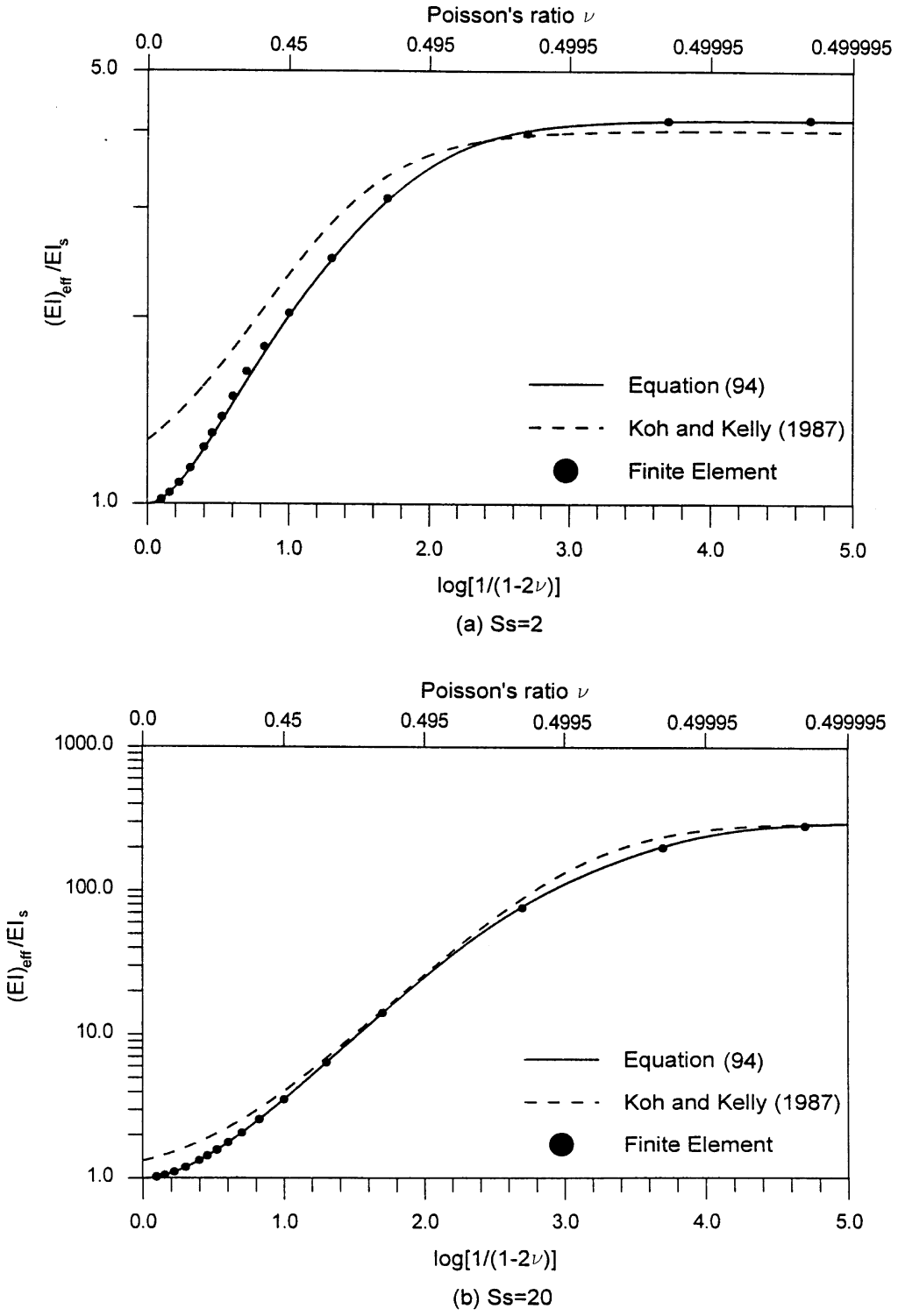


Fig. 9. Effective tilting stiffness of a square layer.

## 6. Conclusion

Based on the two kinematic assumptions, i.e. horizontal planes remain planar and vertical lines become parabolic after deformation, the tilting stiffness of elastic layers bonded between rigid plates are derived through theoretical approach for the layers of infinite-strip, circular and square shapes. For the infinite-strip and circular shapes, the derived tilting stiffness are expressed in close forms. For the square shape, the derived tilting stiffness is expressed in a series form, of which the coefficients must be solved by numerical calculation. However, a simplified close form is also shown to provide good approximation for the tilting stiffness of the square shape.

The tilting stiffnesses calculated by the derived formulae are close to the solutions of the finite element analysis for an extensive range of shape factor and Poisson's ratio. It is also found that when the values of shape factor and Poisson's ratio are high the difference between the tilting stiffness solved by the approach proposed in the present paper and the 'approximate pressure' solution is small. For the infinite-strip shape, the tilting stiffness calculated by the formula derived in the present paper is extremely close to the solution of Lindley (1979b). However, the formula presented herein has a form more compact than the previously published solution.

## Acknowledgement

The research work reported in this paper was supported by the National Science Council, Republic of China, under Grant No. NSC 87-2211-E011-033. This support is greatly appreciated.

## References

Chalhoub, M.S., Kelly, J.M., 1990. Effect of bulk compressibility on the stiffness of cylindrical base isolation bearings. International Journal of Solids and Structures 26, 734–760.

Chalhoub, M.S., Kelly, J.M., 1991. Analysis of infinite-strip-shaped base isolator with elastomer bulk compression. Journal of Engineering Mechanics, ASCE 117, 1791–1805.

Gent, A.N., Lindley, P.B., 1959. The compression of bonded rubber blocks. Proceedings of the Institution of Mechanical Engineers 173, 111–117.

Gent, A.N., Meinecke, E.A., 1970. Compression, bending and shear of bonded rubber blocks. Polymer Engineering and Science 10, 48–53.

Kelly, J.M., 1993. Earthquake-Resistant Design with Rubber. Springer-Verlag, London.

Koh, C.G., Kelly, J.M., 1987. Effects of axial load on elastomeric isolation bearings. Report No. UCB/EERC-86/12. Earthquake Engineering Research Center, University of California, Berkeley.

Lindley, P.B., 1979a. Compression module for blocks of soft elastic material bonded to rigid end plates. Journal of Strain Analysis 14, 11–16.

Lindley, P.B., 1979b. Plane strain rotation moduli for soft elastic blocks. Journal of Strain Analysis 14, 17–21.

Tsai, H.-C., Lee, C.-C., 1998. Compressive stiffness of elastic layers bonded between rigid plates. International Journal of Solids and Structures 35, 3053–3069.